a more detailed discussion and are treated in the following section. In crystals which do have a centre of inversion symmetry, only even-parity vibrations, whose representations have a subscript g, can be Raman active and only odd-parity (subscript u) vibrations can be infra-red active. This fact leads to the important complementary nature of infra-red absorption and Raman effect measurements. Directly above each irreducible representation is a matrix which gives the non-vanishing components of the Raman tensor, i.e. of $\alpha_{\rho\sigma,\,\mu}$ or $R^{\mu}_{\sigma\rho}$. The different elements of the matrices are the nine components of the tensor obtained by allowing both ρ and σ to take on the values x, y and z. Here x, y, and z are the crystal principal axes chosen to be identical with the principal axes x_1, x_2 and x_3 defined for all the crystal classes by Nye (1957). The component μ of the phonon polarization for the case of infra-red-active vibrations is the quantity given in brackets after the irreducible representation symbol. For the unlisted case of triclinic symmetry, the Raman tensor is a general symmetric tensor.

As discussed in the previous section, the Raman tensor is strictly symmetric only when the phonon frequency is neglected in comparison with the radiation frequencies. Ovander (1960) has considered the form of the Raman tensor when this approximation is not made. In addition to the phonon symmetries listed in the table, other types of phonon are now Raman active and the scattering tensor contains in general an anti-symmetric part. The additional Raman lines due to these other types of phonon should be very weak, and we shall assume the Raman tensor to be symmetric throughout the remainder of this article.

The table is used to calculate Raman scattering efficiencies as follows. Let the incident and scattered photons have polarizations in the directions of unit vectors $\mathbf{e}_i$ and $\mathbf{e}_s$ respectively. The scattering efficiency is given by:

$$S = A\left[\sum_{\rho,\,\sigma=x,\,y,\,z} e_i^{\sigma} R_{\sigma\rho} e_s^{\rho}\right]^2, \qquad \ldots\ldots \quad (36)$$

where A is a constant of proportionality and e_i^{σ} and e_s^{ρ} are components of the unit vectors along the principal axes σ and ρ. For two- or three-fold degenerate phonons the contributions of the two or three matrices given in the table are added to find the total scattering efficiency. As examples of the use of the tables, we consider the scattering geometry shown in fig. 5. For the B phonon symmetry in the C_4 group, the Raman efficiency for scattered light polarized in the plane of scattering (i.e. the xz-plane) is:

$$S_{\parallel} = A(e_i^x c + e_i^y d)^2 \cos^2\psi \qquad \ldots\ldots \quad (37)$$

and for scattered light polarized perpendicular to the plane of scattering is:

$$S = A(e_i^x d - e_i^y c)^2, \qquad \ldots\ldots \quad (38)$$

where the scattered light has been assumed to be approximately transverse even for the extraordinary ray. For the F_{2g} vibration in the O_h group,

the analogous quantities are:

$$S_{\parallel} = Ad^2[(e_i^x \sin\psi)^2 + (e_i^y)^2], \quad . \quad . \quad . \quad . \quad . \quad . \quad . \quad (39)$$

$$S_{\perp} = Ad^2(e_i^x)^2. \quad . \quad . \quad . \quad . \quad . \quad . \quad . \quad . \quad . \quad . \quad (40)$$

When $\psi = \pi/2$ the sum of $S_{\parallel}$ and $S_{\perp}$ contains three terms which are the same three as occur in (31).

Experimentally it is more common to keep the directions of incident and scattered light fixed at right-angles to each other and to vary the orientation of the crystal axes relative to the light directions. A special

Fig. 6

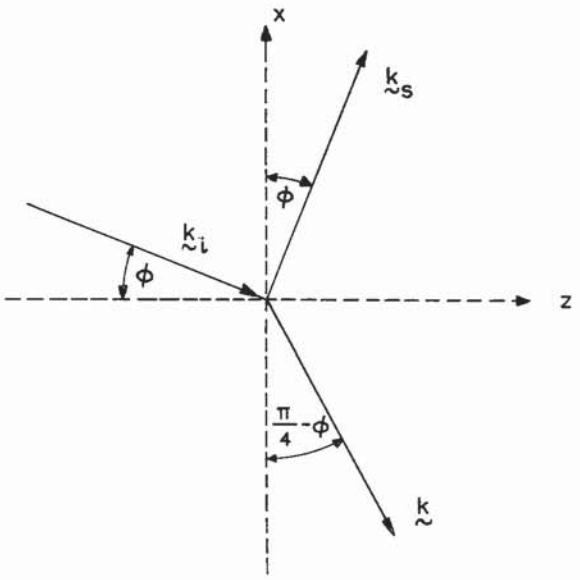

Alternative Raman scattering geometry.

case of this geometry is shown in fig. 6. As an example, consider a phonon of A_1 symmetry in the group D_4 or D_6. The scattering efficiencies are:

$$S_{\parallel} = A[e_i^x a \sin\phi - e_i^z b \cos\phi]^2 = A(e_i^{\parallel})^2 \tfrac{1}{4}(a-b)^2 \sin^2 2\phi, \quad . \quad . \quad (41)$$

$$S_{\perp} = A(e_i^y a)^2 = A(e_i^{\perp} a)^2, \quad . \quad . \quad . \quad . \quad . \quad . \quad . \quad . \quad . \quad . \quad (42)$$

where $e_i^{\parallel}$ and $e_i^{\perp}$ are the components of $\mathbf{e}_i$ parallel and perpendicular to the plane of scattering (the light waves are assumed transverse). These last equations have been derived and discussed by Poulet (1955).

An important quantity, usually defined for scattering through a right-angle as in fig. 6, is the depolarization ratio ρ. This is defined to be the ratio of the intensity of the component of scattered radiation polarized parallel to the plane of scattering to the intensity of the component polarized

perpendicular to the scattering plane. Expressed in terms of scattering efficiencies:

$$\rho = \frac{S_{\parallel}}{S_{\perp}}. \quad . \quad . \quad . \quad . \quad . \quad . \quad . \quad . \quad . \quad . \quad (43)$$

The depolarization ρ evidently depends on the angle ϕ, and its magnitude and angular variation provide important information for deciding the symmetry type of an observed Raman line. Only the A and E symmetry vibrations in cubic crystals produce scattered light with a depolarization ratio ρ independent of ϕ. Saksena (1940) has tabulated theoretical depolarization ratios for many crystal symmetries and for three different states of polarization of the incident light; he considers both forward (longitudinal) and right-angle (transverse) scattering. Whereas Saksena's results are restricted to light propagated along principal axes, Chandrasekharan (1963) has calculated the Raman scattering matrix for cubic crystals for any arbitrary relative orientations of crystal axes, incident-light wave vector and scattered-light wave vector.

Finally, we mention that Theimer (1955, 1956) in attempting to remove difficulties in the interpretation of measured intensities and depolarization ratios in calcite, has proposed that in some cases the appropriate symmetry group to use is not that of the crystal lattice but only its sub-group of operations which leave the phonon wave vector **k** invariant. We feel that the validity of this approach has not been established.

2.4. *Extensions of the Theory for Piezo-electric Crystals*

The theories reviewed so far provide an adequate basis for interpreting the first-order Raman spectra produced by scattering from non-polar lattice vibrations. However, extensions of the theory are necessary to deal with scattering from lattice vibrations which are simultaneously Raman and infra-red active. Experimentally, this type of scattering was regarded as anomalous, until its features were explained theoretically by Poulet (1955). The scattering is 'anomalous' in two ways:

(1) More first-order Raman peaks are observed than would be expected on the basis of a group-theoretical treatment of the symmetries of the vibrations. This is due to a lifting of the group-theoretical degeneracy of polar lattice vibrations by long-range electrostatic forces as discussed in § 2.1 and illustrated in figs. 1, 2 and 3. In these figures, the group-theoretical degeneracy is that existing at $k = 0$, while the phonon frequencies observed in the Raman effect are those at the right-hand edges of the figures. In uniaxial crystals, some of the Raman frequencies show an angular dependence. All these features have been fully discussed in § 2.1.

(2) The experimental magnitudes and angular dependencies of the scattering efficiencies and depolarization ratios are not in agreement with the theoretical expressions given in §§ 2.2 and 2.3, even when the lifting of group-theoretical degeneracies is taken into account. This is again due to the long-range electric fields associated with the polar vibrations. The

electric fields give rise to an electron-lattice interaction additional to the deformation potential type, and this interaction varies with phonon direction due to the variation in field strength.

In this section we review the theory of these anomalies. It is convenient to divide the discussion into two parts, for cubic and uniaxial crystals.

(i) *Cubic crystals.* As discussed in § 2.1.1, the threefold Raman and infra-red-active vibration in a cubic crystal splits into two vibrations, one transversely and the other longitudinally polarized. Consider, for example, the F_2 vibration in a crystal of T_d symmetry, a case treated by Poulet (1955). In the previous section we have calculated the scattering efficiencies from the analogous vibration in a crystal with inversion symmetry (F_{2g} in O_h) using the basic eqn. (36). According to this equation the scattering efficiency is obtained by adding the contributions of the three matrices given in the table. However, when the threefold degeneracy is lifted it is necessary to take account of the fact that the three matrices correspond to polarization components of the phonon along the three principal axes, and these components can no longer all be chosen to be unity. It is thus necessary to generalize (36) by introducing a unit vector $\boldsymbol{\xi}$ in the direction of the mechanical polarization of the phonon. The formula for the scattering efficiency then becomes:

$$S = A\left[\sum_{\substack{\rho,\sigma,\tau \\ =x,y,z}} e_i^{\sigma} R_{\sigma\rho}^{\tau} \xi^{\tau} e_s^{\rho}\right]^2, \qquad \ldots\ldots \quad (44)$$

where τ is given in brackets in the table after the appropriate irreducible representation symbols. The contributions of the three matrices in the table for a phonon of given polarization are now summed before taking the square in (44).

For a threefold degenerate vibration like F_{2g} in O_h, (44) gives a result identical to that given by (36). However, for the F_2 vibration of T_d, assuming the scattering geometry of fig. 5, the longitudinal vibration gives scattering efficiencies:

$$S_{\parallel}^{l} = A' d^2 (e_i^y \sin 3\psi/2)^2, \qquad \ldots\ldots \quad (45)$$

$$S_{\perp}^{l} = A' d^2 (e_i^x \sin \psi/2)^2. \qquad \ldots\ldots \quad (46)$$

For the transverse vibration, the contributions to the scattering by phonons polarized parallel and perpendicular to the scattering plane add to give:

$$S_{\parallel}^{t} = A d^2 [(e_i^y \cos 3\psi/2)^2 + (e_i^x \sin \psi)^2], \qquad \ldots\ldots \quad (47)$$

$$S_{\perp}^{t} = A d^2 (e_i^x \cos \psi/2)^2. \qquad \ldots\ldots \quad (48)$$

Note that $S_{\parallel}^{l} + S_{\parallel}^{t} = S_{\parallel}$ given by (39) and $S_{\perp}^{l} + S_{\perp}^{t} = S_{\perp}$ given by (40) provided that $A = A'$. Results equivalent to eqns. (45) to (48) have been given by Ovander (1962 a), who calculated the form of the Raman tensor for this case by direct expansion of the electronic wave-functions in a power series in the phonon displacement coordinates, as is done in the Born theory of Raman scattering by non-polar lattice vibrations. Ovander has drawn

attention to the fact that the scattering efficiencies for the transverse and longitudinal phonons are not symmetrical about $\psi = \pi/2$, in contrast to the scattering efficiency for the threefold degenerate vibration; the transverse vibration gives greater scattering in forward directions, and the longitudinal vibration in backward directions. Poulet (1955) has given formulae for the intensities and depolarization ratios of light Raman scattered through a right-angle by cubic crystals having various orientations with respect to the light beams.

The constant of proportionality for scattering by the longitudinal vibration in (45) and (46) has been distinguished by a prime from the constant occurring in (47) and (48) for scattering by the transverse vibration. That the two constants should be different was first noted experimentally by Couture-Mathieu and Mathieu (1953) and the phenomenon was subsequently explained theoretically by Poulet (1955). It is due to the fact that the electric field accompanying a polar lattice vibration provides an additional electron–lattice interaction mechanism. This mechanism is well known in the realm of electron transport theory in the group III–V semiconductors, where it is known in some cases to lead to a stronger electron–phonon coupling than the deformation potential interaction (Ehrenreich 1957). In making a calculation of the Raman scattering produced by this additional mechanism, it is necessary to decide whether the electrons in the crystal experience the macroscopic field $\mathbf{E}_{\mathrm{mac}}$ or the local field $\mathbf{E}_{\mathrm{local}}$ produced by the polar phonon. The two fields are related by:

$$\mathbf{E}_{\mathrm{local}} = \mathbf{E}_{\mathrm{mac}} + \frac{4\pi}{3}\mathbf{P}, \quad . \quad . \quad . \quad . \quad . \quad . \quad . \quad . \quad (49)$$

where $\mathbf{P}$ is the polarization. It has been shown in § 2.1 that the transverse phonon has $\mathbf{E}_{\mathrm{mac}} = 0$, while the longitudinal phonon has $\mathbf{E}_{\mathrm{mac}}$ given by (6). Thus if the electrons of importance in the Raman effect experience $\mathbf{E}_{\mathrm{mac}}$, the additional scattering mechanism occurs only for the longitudinal phonons. This is the point of view adopted by Ovander (1962 a) and Loudon (1963 b) and in the transport theory of polar semiconductors. However, Poulet (1955) assumes that the electrons experience $\mathbf{E}_{\mathrm{local}}$, which leads to additional scattering for both transverse and longitudinal phonons. The calculations of Darwin (1934) and Nozières and Pines (1958) show that $\mathbf{E}_{\mathrm{mac}}$ should be used in crystals where the electrons are not localized on individual atoms (e.g. semiconductors), whereas $\mathbf{E}_{\mathrm{local}}$ should be used for crystals where the electrons are tightly bound to the atoms.

Explicit calculations of the Raman scattering produced by the polar interaction have been fully carried out only for the phonons in the zinc blende lattice. There are two methods of calculation corresponding to the two methods of obtaining the non-polar scattering efficiency described in § 2.2. Poulet (1955) has extended the Born and Bradburn method by expanding the polarizability $\alpha_{\rho\sigma}$ in a power series similar to (23), but with terms in the phonon electric field included, in addition to the terms in the phonon displacement $\mathbf{r}$. For cubic crystals both the phonon displacement

and electric field point in the same direction, so that the symmetries of the scattering produced by the two electron–lattice interactions are identical. In the expansion of $\alpha_{\rho\sigma}$, the term linear in the electric field has as its coefficient the rate of change of polarizability with applied electric field. This quantity can be related to the linear electro-optic coefficients of the crystal (see Nye 1957), for the change in the component $\epsilon_{\mu\nu}$ of the optical dielectric constant tensor $\boldsymbol{\epsilon}$ produced by an electric field $\mathbf{E}$ is:

$$\delta\epsilon_{\mu\nu} = -\sum_{\rho,\sigma}\sum_{\tau}\epsilon_{\mu\rho}z_{\rho\sigma,\tau}\epsilon_{\sigma\nu}E_{\tau}, \qquad . \quad . \quad . \quad . \quad . \quad (50)$$

where $z_{\rho\sigma,\tau}$ is an electro-optic coefficient. The calculation thus leads to an expression for the polar Raman scattering which depends only on quantities which can be measured by independent experiments.

A similar result has been derived by Loudon (1963 b), who calculated the scattering efficiency by third-order perturbation theory using (30) but with H_{EL} representing now the polar electron–lattice interaction. The scattered amplitude can be related to a microscopic expression for the electro-optic coefficients if the phonon frequency is negligible in comparison to the light frequencies. For a zinc blende type lattice, assuming the scattering geometry of fig. 5 with $\psi = \pi/2$, and taking the case where the electrons experience $\mathbf{E}_{\mathrm{mac}}$, the scattering efficiency for the transverse vibration using unpolarized incident light is obtained from (31), (47) and (48):

$$S_t = \frac{e^4 V(n_0+1)Ld\Omega}{2\hbar^3 m^4 d^2 Mc^4\omega_0}|R^z_{xy}|^2, \qquad . \quad . \quad . \quad . \quad . \quad . \quad (51)$$

where the difference between the incident and scattered light frequencies has been ignored. For the longitudinal vibration, the calculation of Loudon gives a total scattering efficiency:

$$S_l = \frac{\hbar\omega_l(n_l+1)Ld\Omega}{4\pi c^4}\left|\frac{e^2}{\hbar^2\omega_l m^2 d}\left(\frac{\pi V}{M}\right)^{1/2}R^z_{xy} - \frac{\omega_i^2\epsilon^2}{2}\left(\frac{1}{\epsilon}-\frac{1}{\epsilon^0}\right)^{1/2}z_{41}\right|^2, \quad . \quad (52)$$

where n_l is the Bose–Einstein factor for the longitudinal phonons of frequency ω_l, and z_{41} is the electro-optic coefficient for the zinc blende lattice in condensed notation (see Nye 1957). The calculation of Poulet (1955) using $\mathbf{E}_{\mathrm{local}}$ gives a result in which both S_t and S_l contain a term in z_{41} Since R^z_{xy} is the only factor in (51) and (52) which cannot be otherwise measured, it should in principle be possible to determine which electric field acts on the electrons by measuring the relative intensities of the two Raman peaks and the incident light. Such an experiment would however be difficult in practice and there is little or no information in the literature on the relative intensities of incident and scattered radiation.

A different approach to the calculation of Raman scattering intensities has been followed by Ovander (1962 b) and the method has been applied to cubic crystals by Grechko and Ovander (1962). In this method the crystal is regarded as a collection of interacting molecules and that part of the interaction between the radiation and the molecules which mixes the molecular electronic excited states with the ground state is diagonalized.

The resulting eigenstates are mixtures of radiative and electronic excitations (polaritons). Ovander now considers three terms in the Hamiltonian which can cause Raman scattering from molecular vibrational levels. The part of the electron–radiation interaction which mixes two molecular excited states together is denoted H_A and gives a Raman scattering equivalent to that of § 2.2 when the deformation potential electron-lattice interaction is inserted. The term arising from the $e^2A^2/2mc^2$ part of the electron-radiation interaction (denoted H_B) leads to significant Raman scattering only for incident radiation in the x-ray region (see Peierls 1955 for a discussion of this type of scattering), and it is neglected by Ovander. Finally the intermolecular interaction term leads to a Raman scattering Hamiltonian H_C (called H_B in Ovander's later papers); when H_C arises from the interactions of the electronic and vibrational dipole moments of all the molecules in the crystal, the Hamiltonian produces the part of the Raman scattering due to the polar electron–lattice interaction already discussed in this section. Grechko and Ovander (1962) show that this method of calculation leads to the expressions for the angular dependence of the scattering already given.

When the frequency ω_i of the incident light approaches one of the electronic excitation frequencies of the crystal, terms in the Raman tensor diverge, as is evident from (32). Ovander (1962 b, c) has discussed this so-called resonance Raman scattering in terms of his theory outlined above. The divergence is removed by a proper consideration of the electron–radiation interaction in the region of the resonance. Loudon (1963 b) has treated resonance scattering for a situation where ω_i is close to the forbidden energy gap frequency in an insulator. The Raman tensor is always finite in this case even using (32) without modification, due to the arrangement of the electronic energy levels in bands.

(ii) *Uniaxial crystals.* As discussed in § 2.1.2, a polar uniaxial crystal having two atoms in the unit cell may have three infra-red-active lattice vibration branches, two of the branches being degenerate for propagation parallel to the c-axis, one of these and the remaining branch having a frequency which depends on the direction of propagation. The angular dependence of the Raman scattering efficiences can be calculated using the results of § 2.3 modified to take the effect of the long-range electric forces into account.

Let us consider the example of a crystal having C_{4v} symmetry. Reference to the table shows that group theoretically an infra-red and Raman-active phonon can be non-degenerate of type A_1 corresponding to lattice displacements parallel to the c-axis or twofold degenerate of type E corresponding to lattice displacements perpendicular to the c-axis. The long-range electric forces lift the twofold degeneracy and mix the A_1 and E symmetry phonons, so that for a general direction of propagation there are three non-degenerate types of phonon, two of which have neither purely A_1 nor purely E symmetry. Thus all three A_1 and E matrices contribute in general to the Raman scattering efficiency for two of the three phonon branches.

In addition to this feature, the formula (44) for the scattering efficiency must be further generalized to take account of the two types of electron–lattice interaction. In uniaxial crystals the lattice displacement $\mathbf{r}$ (parallel to $\boldsymbol{\xi}$), which controls the deformation potential scattering, is not in general parallel to the electric field $\mathbf{E}$ (parallel to $\mathbf{k}$), which controls the polar scattering. Following the calculation of Poulet (1955), described in part (i) of this section, in which the Born and Bradburn method is extended by inclusion of terms in both $\mathbf{r}$ and $\mathbf{E}$ in the expansion of the polarizability $\alpha_{\rho\sigma}$, it is seen that (44) must be generalized to:

$$S=\left\{\sum_{\substack{\rho,\sigma,\tau\\=x,y,z}} e_i^{\sigma} R_{\sigma\rho}^{\tau}(\alpha\xi^{\tau}+\beta\hat{k}^{\tau})e_s^{\rho}\right\}^2, \qquad (53)$$

where β is proportional to the electric field strength $|\mathbf{E}|$. The contributions of the three matrices in the table corresponding to polarization components in the x, y and z directions must be summed before taking the square in (53) (for symmetry groups D_3, D_4, C_{3h}, D_6 and D_{3h} there are only two matrices in the table, corresponding to polarization components in the x and y directions). We may note that (53) contains (44) as a special case. For cubic crystals, where $\boldsymbol{\xi}$ and $\hat{\mathbf{k}}$ point in the same direction for longitudinal vibrations, the constant of proportionality is $(\alpha+\beta)^2$, equal to A' in (45) and (46); for transverse vibrations, where β is zero, the constant of proportionality is α^2, equal to A in (47) and (48). In both cubic and uniaxial crystals β is always zero for exactly transverse branches.

Consider first a crystal of the type discussed in part (i) of § 2.1.2 (electrostatic forces predominant over anisotropy in the short-range interatomic forces). These crystals have a quasi-longitudinal extraordinary phonon for which the almost constant electric field $\mathbf{E}$ and the atomic displacement $\mathbf{r}$ are approximately collinear. Assuming the geometry of fig. 5, and taking the scattered light to be approximately transverse, the scattering efficiencies for this phonon for a crystal of C_{4v} symmetry are:

$$S_{\parallel}=\{e_i^x a\sin\psi/2\cos\psi+e_i^x e\cos\psi/2\sin\psi\}^2(\alpha+\beta)^2, \qquad (54)$$

$$S_{\perp}=\{e_i^y a\sin\psi/2\}^2(\alpha+\beta)^2. \qquad (55)$$

The quasi-transverse extraordinary phonon has negligible electric field, leading to:

$$S_{\parallel}=\{e_i^x a\cos\psi/2\cos\psi-e_i^x e\sin\psi/2\sin\psi\}^2\alpha^2, \qquad (56)$$

$$S_{\perp}=\{e_i^y a\cos\psi/2\}^2\alpha^2, \qquad (57)$$

while the transverse ordinary phonon finally gives:

$$S_{\parallel}=\{e_i^y e\sin\psi\}^2\alpha^2, \qquad (58)$$

$$S_{\perp}=0. \qquad (59)$$

For polar uniaxial crystals of the type discussed in part (ii) of § 2.1.2 (anisotropy of the short-range interatomic forces predominant over electrostatic forces), the calculation of the Raman scattering efficiency from phonons which are infra-red active is a little more complicated.

For these vibrations, the two extraordinary phonons have a lattice displacement **r** directed approximately parallel or perpendicular to the c-axis, while the electric field **E** is parallel to **k**, as in (20) and (21). In addition, these equations show that the electric field strength itself has a strong angular dependence. These features lead to different angular dependences for the contributions to the scattering resulting from the deformation potential and polar electron–lattice interactions. We again assume a crystal of C_{4v} symmetry with the scattering geometry of fig. 5. Consider first the extraordinary phonon associated with lattice displacements parallel to the c-axis, whose frequency and electric field strength are given by (18) and (20), i.e. the upper branch of fig. 3. The scattering efficiencies are:

$$S_{\parallel} = \{e_i^x a\,[\alpha + \beta \sin^2 \psi/2] \cos\psi + e_i^x e \beta \sin\psi/2 \cos\psi/2 \sin\psi\}^2, \quad . \quad (60)$$

$$S_{\perp} = \{e_i^y a[\alpha + \beta \sin^2 \psi/2]\}^2, \quad . \quad . \quad . \quad . \quad . \quad . \quad . \quad . \quad . \quad . \quad . \quad (61)$$

where the $\sin \psi/2$ dependence of β has been displayed explicitly. This result (with a $\cos\psi$ factor omitted) has been obtained by Ovander (1962 d) using his method of calculation outlined above. The second extraordinary phonon has its lattice displacement approximately parallel to the x-axis; the frequency and electric field of this branch are given by eqns. (19) and (21). The scattering efficiencies are:

$$S_{\parallel} = \{e_i^x a\beta \cos\psi/2 \sin\psi/2 \cos\psi - e_i^x e[\alpha - \beta \cos^2 \psi/2] \sin\psi\}^2, \quad . \quad (62)$$

$$S_{\perp} = \{e_i^y a\beta \cos\psi/2 \sin\psi/2\}^2. \quad . \quad . \quad . \quad . \quad . \quad . \quad . \quad . \quad . \quad . \quad . \quad (63)$$

There is a small additional angular variation in these last four equations due to the dependence of the phonon frequency on angle, since the equations for S contain this frequency as a factor (cf. the corresponding eqns. (51) and (52) for the cubic case). Finally, the scattering efficiencies for the ordinary phonon are the same as those given previously in eqns. (58) and (59). Ovander (1962 d) has also given results for these last two branches.

Poulet (1955) has derived results for Raman scattering by the phonon whose lattice displacements are parallel to the c-axis, in the geometry of fig. 6. Poulet uses again the local field of the lattice vibration, whereas the results of this section have assumed the macroscopic field to be the appropriate one. The latter assumption gives:

$$S_{\perp} = \{e_i^{\perp} a[\alpha + \beta \sin^2 (\pi/4 - \phi)]\}^2, \quad . \quad . \quad . \quad . \quad (64)$$

while $S_{\parallel}$ is rather complicated and will not be written down. In fact, Poulet's calculation refers to a C_{6v} symmetry crystal, but the appropriate tensors have the same symmetry. The corresponding non-polar A_1 vibration, in crystal of D_4 or D_6 symmetry, has already been treated in (41) and (42).

There have been no calculations of the constants of proportionality occurring in the equations for the scattering efficiency in uniaxial crystals, analogous to (51) and (52) for cubic crystals. It would not be difficult to make such a calculation for a specific crystal symmetry. The polar part of the scattering would again lead to terms proportional to electro-optic

coefficients when the phonon frequency could be neglected in comparison with ω_i and ω_s.

2.5. *Temperature Effects*

There have been several experimental studies of the dependence of Raman spectra on temperature. Both the Raman shifts and linewidths, and also the scattered intensities vary with temperature.

The variation with temperature of the shifts and widths of Raman lines has been measured in quartz by Nedungadi (1940), in diamond by Krishnan (1946a), in calcite and quartz by Narayanaswamy (1947), and in topaz by Srinivasan (1953). The common features are a broadening of the Raman lines with increase in temperature accompanied by a shift of the Stokes lines to higher frequencies. The amount of temperature shift is different for different Raman lines, being in general larger for the lines of higher frequency. That is, the phonon frequencies decrease with increasing temperature, the decrease being larger the smaller the phonon frequency.

These features can be qualitatively understood in terms of the anharmonic forces in the crystal lattice. The width and temperature shift of the Raman lines are the same as the phonon width and shift which are observed experimentally in other types of experiment, e.g. neutron scattering or infra-red absorption by phonons, and theoretical expressions for them can be derived quantum mechanically. Inclusion of anharmonic forces leads to the replacement of the total scattering efficiency S, given for example by (31), by a scattering efficiency $S(\omega_s)\,d\omega_s$ defined in terms of the fractional number of incident photons converted into scattered photons having their frequencies in a range $d\omega_s$ about ω_s. This efficiency can be shown to satisfy the relation:

$$S(\omega_s) = \frac{S}{\pi}\frac{\Gamma}{(\omega_i-\omega_0-\omega_s-\Delta)^2+\Gamma^2}. \quad . \quad . \quad . \quad . \quad . \quad . \quad (65)$$

The Raman scattered radiation thus has a Lorentzian distribution about the frequency $\omega_i-\omega_0-\Delta$ with a half-width Γ. The total scattering efficiency is still the quantity S, since

$$\int S(\omega_s)\,d\omega_s = S. \quad . \quad . \quad . \quad . \quad . \quad . \quad . \quad . \quad (66)$$

Quantum-mechanical expressions for the shift Δ and half-width Γ due to third-order anharmonic forces have been given by Maradudin *et al.* (1962). Fourth-order anharmonic forces may also make significant contributions to Γ and Δ at high temperatures. The expressions for Γ and Δ are too complicated to be evaluated explicitly except for simplified lattice models. However, from the form of the expressions it is clear that the magnitudes of both Γ and Δ should increase with temperature, the dependence on temperature being linear when $k_B T/\hbar$ is much greater than the phonon frequencies. This agrees with the experimental results, which show a linear dependence of Γ and Δ on temperature at sufficiently high temperatures. In fact the

change of phonon frequency with temperature is due not only to the anharmonic coupling of the Raman phonons to other vibrations, but also to the thermal expansion of the lattice (see Maradudin 1962 and Maradudin and Fein 1962). A complete discussion of Δ and its temperature variation must take this factor into account. Viswanathan (1963) has also derived expressions for the width and temperature shift of Raman lines; his results do not appear to agree with those of the authors cited above.

The theoretical scattered intensities and efficiences also depend on temperature, by a factor n_0+1 for Stokes lines and a factor n_0 for anti-Stokes lines. There have been several experimental investigations of the temperature dependence of the intensities of Stokes lines. Bobovich and Tulub (1959, 1960) have investigated nine types of crystal, including quartz, calcite and CaF_2, and these last three crystals have been subsequently re-studied by Stekhanov and Chisler (1962). Stekhanov (1955) has measured temperature-dependent intensities in gypsum. The experiments require care and some of the earlier measurements produced spurious results (see the criticism of earlier work in Stekhanov and Chisler 1962). The lines studied have an intensity which either increases at the theoretical rate or increases more slowly than predicted, except for one of the Raman lines in quartz which appears to increase more rapidly than the theory predicts. The falling of the intensity below that expected theoretically in some cases is not entirely understood. Some of the loss as the sample is heated may be due to the increasing breadth of the Raman lines which causes a progressively larger fraction of the line intensity to move out into the wings of the line and escape detection. Theimer (1956) has suggested that departures of the temperature dependence from the theoretical (n_0+1) factor may be due to more complicated Raman scattering processes in which an extra step involving the creation and destruction of a virtual phonon occurs. This type of process is made possible by the existence of third-order anharmonic forces in the lattice.

2.6. *Experimental Results*

A list of experimental work is given in a separate group of references at the end of the article. The list is not completely exhaustive and references to some of the work on more complex crystals (e.g. sulphates and hydroxides) has been omitted. In much of this work only a few of the Raman-active vibrations are observed and no interpretation of the measurements is possible. Of the work which is listed some of the more interesting measurements are singled out here for discussion.

2.6.1. *Piezo-electric crystals*

Mathieu and his collaborators have published a series of papers containing the results of measurements on piezo-electric crystals, and the theoretical work of Poulet (1955) reviewed in § 2.4 is based upon some of the earlier measurements in the series. Couture-Mathieu, Poulet and Mathieu (1952) have measured the Raman spectra of $NaClO_3$ and $NaBrO_3$. These

crystals belong to the cubic symmetry group T, and the longitudinal and transverse vibrations of type F exhibit values of the depolarization ratio which can be quite well accounted for by the theory of Poulet, but which were thought to be anomalous before the important theoretical modifications required for piezo-electric crystals were fully understood. A similarly good agreement with theory is obtained for the case of ZnS in the zinc blende structure (Couture-Mathieu and Mathieu 1953). The lattice has T_d symmetry with single transverse and longitudinal optic vibrations of F_2 symmetry, whose measured frequencies (274 cm^{-1} and 349 cm^{-1} respectively) are in good agreement with the Lyddane–Sachs–Teller relation (Poulet 1954, 1955). Recent measurements on CuCl (Mathieu *et al.* 1960), which has the same structure, have only resolved a single Raman line, presumably that of the longitudinal optic branch which in the case of zinc blende is ten times more intense than the line due to the transverse optic branch. Thus in both ZnS and CuCl the scattering produced by the polar electron–lattice interaction appears to dominate that produced by the deformation potential interaction.

For the case of uniaxial crystals, the theory of § 2.4 has been compared with the Raman spectrum of lithium perchlorate hydrate measured by Mathieu and Couture-Mathieu (1952 a). The crystal has symmetry class C_{6v} and the vibrations of symmetries A_1 and E_1 are both Raman and infra-red active. One of the observed Raman peaks exhibits a frequency which depends on crystal orientation, following a relation similar to (18). This vibration has thus been assigned to the A_1 symmetry type by Poulet, who has also shown that the variation of Raman intensity with orientation may be represented by an equation similar to (64). One of the other Raman peaks also has a frequency variation which appears to follow eqn. (18).

Other measurements in the series by Mathieu and co-workers have detected angular dependencies of the Raman peaks which can be interpreted in terms of Poulet's theory for piezo-electric crystals (see Mathieu and Couture-Mathieu 1952 b, Weil and Mathieu 1954, Mathieu *et al.* 1955, Poulet and Mathieu 1956). Haas and Hornig (1959) have collected together many of the values of transverse and longitudinal frequencies measured by Mathieu and his co-workers.

2.6.2. *Quartz*

In the period under review there have been more measurements of the Raman spectrum of quartz than of any other crystal. Quartz has a strong Raman spectrum with a number of well-resolved lines. The crystal symmetry group of α-quartz is D_3 and there are three SiO_2 groups in the unit cell leading to four A_1 and eight E vibrations which can contribute to the Raman spectrum. The remaining degrees of freedom are taken up by the three acoustic modes and four infra-red-active A_2 vibrations. The E vibrations are also infra-red active and the resulting angular dependencies of the frequencies and intensities of some of the E vibrations have been

observed by Mathieu and Couture-Mathieu (1952 b). A recent re-measurement of the Raman spectrum of quartz has been made by Krishnamurti (1958). Zubov and Osipova (1961) have made careful measurements of the widths and shapes of 11 lines in the Raman spectrum of quartz at room temperature; they find that all the lines have a shape close to Lorentzian with widths ranging from 4 cm^{-1} to 21 cm^{-1}. The same authors (Zubov and Osipova 1962) have shown that neutron irradiation of α-quartz produces shifts and increased breadths of the Raman lines, and Zubov *et al.* (1962) have observed small intensity changes in two of the Raman lines when an electric field is applied to the crystal.

The infra-red lattice bands of α-quartz have been measured by Spitzer and Kleinman (1961) and the observed E vibrations have been compared with the same vibrations observed in Raman scattering. These same authors (Kleinman and Spitzer 1962) have made a theoretical study of the four A_1 and four A_2 optical vibrations, obtaining good agreement with experiment.

The Raman spectrum of vitreous silica has been measured by Krishnan (1953) and Flubacher *et al.* (1959). The two measurements give results which agree in their general features. The spectrum exhibits broad bands rather than sharp peaks and its most striking feature is an intense continuum which extends from shifts of 8 cm^{-1} to 560 cm^{-1}. The spectrum of vitreous silica is thus markedly different from that of α-quartz.

2.6.3. *Alkaline-earth fluorides*

These crystals have recently become important as host lattices for rare earth ions used in producing laser emission. The spectral lines due to electronic transitions of rare earth ions in crystals frequently exhibit side bands, due to transitions in which phonons are simultaneously created or destroyed, and the displacements of the side bands give information about the lattice vibration frequencies. The phonon-assisted transitions are known as vibronics. The fluorides have symmetry group O_h with one group of three atoms in the unit cell, leading to one Raman-active F_{2g} optic branch and one infra-red-active F_{1u} branch. Wood and Kaiser (1962) have measured the absorption and fluorescence spectra of Sm^{2+} in CaF_2, SrF_2 and BaF_2. For SrF_2 they find that one of the vibronic side bands has a shift of 282 cm^{-1}, which is close to the shift of 280 cm^{-1} of the single strong line in the Raman spectrum of SrF_2 measured by Richman (1964). For BaF_2, the corresponding vibronic shift is 244 cm^{-1}, which compares with the Raman shift measured by Krishnan and Narayanan (1963) to be 244 cm^{-1} and by Richman (1964) to be 243 cm^{-1}. For CaF_2 the Raman shift observed by Ananthanarayanan (1962) is 322 cm^{-1}, but Wood and Kaiser do not see any vibronic shift close to this frequency.

Mention may also be made of the measurements of Richman *et al.* (1963), who have correlated the Raman spectrum of $LaCl_3$ with the vibronic transitions of Pr^{3+} in $LaCl_3$.

2.6.4. *Wurtzite structure crystals*

The wurtzite lattice has C_{6v} symmetry and is one of the simplest structures of uniaxial crystal, being obtained from the cubic zinc blende (T_d) lattice by a rearrangement of the planes of atoms perpendicular to the (111) axis (Birman 1959). There are four atoms in the unit cell, leading to single A_1 and E_1 optic branches which are both Raman and infra-red active, two E_2 branches which are Raman active, and two inactive B branches in addition to the A_1 and E_1 acoustic branches. The Raman spectra of SiC and ZnS having the wurtzite structure have been measured. Both these crystals occur also in cubic T_d symmetry modifications, and individual atoms have the same nearest neighbour configuration in both structures leading to some similarities in the phonon spectra. Merten (1962) has discussed the modifications in the phonon spectra on changing from a zinc blende to a wurtzite lattice in terms of a halving of the Brillouin zone dimension in the (111) direction. The main effect of the transition is then a folding back of the phonon branches at the new zone boundary, frequencies which previously occurred at the symmetry point L in the zinc blende Brillouin zone now occurring at the centre of the wurtzite Brillouin zone. The anisotropy in the interatomic forces for these wurtzite structure crystals is very small, and the discussion of § 2.1.2, part (i) applies, the angular dependence of the phonon frequencies being small, as illustrated in fig. 2.

The Raman spectrum of SiC has been measured by Mathieu and Poulet (1957), but the interpretation which they give must be modified in the light of a subsequent measurement of the infra-red properties of SiC by Spitzer, Kleinman and Walsh (1959). The Raman measurements were made with incident light directed parallel to the c-axis and scattered light viewed at right angles. The line observed at 797 cm^{-1} is close to the ordinary absorption resonance frequency observed by Spitzer *et al.* and must have E_1 symmetry. The Raman lines observed at 789 cm^{-1} and 966–969 cm^{-1} (the doublet nature of this line is not accounted for) are evidently due to the transverse-like and longitudinal-like phonons of intermediate A_1–E_1 symmetry. The former frequency is close to the extraordinary ray resonance frequency observed by Spitzer *et al.* (for light propagated perpendicular to the c-axis) and the latter frequency is close to that predicted by the Lyddane–Sachs–Teller relation. For SiC accordingly, $\omega_{\parallel}$ is smaller than $\omega_{\perp}$, opposite to the relative values assumed for fig. 2. The remaining Raman lines at 335 cm^{-1} and 764 cm^{-1} can now be assigned to the two E_2 phonons. Spitzer, Kleinman and Frosch (1959) have measured the ordinary ray resonance frequency in *cubic* SiC and find it to be equal to the corresponding frequency in the *hexagonal* (wurtzite) form of SiC.

Mathieu *et al.* (1963) have measured the Raman spectrum of ZnS in the wurtzite structure. They observed three of the first-order Raman-active phonons, two of the observed frequencies being equal to the frequencies of the transverse and longitudinal optic phonons in cubic ZnS, and thus of A_1–E_1 symmetry. The remaining peak at 217 cm^{-1} is evidently due to a phonon of E_2 symmetry.

2.6.5. *Ferro-electric crystals*

The Raman spectra of several ferro-electric crystals have been measured. Such crystals are particularly interesting for Raman measurements because the lattice symmetry changes when the crystal is cooled through its transition temperature, leading to corresponding changes in the spectra. Thus in Rochelle salt, Stekhanov and Gabrichidze (1963) have observed changes in Raman shifts and intensities when the crystal passes from its D_{2d} para-electric state to its C_2 symmetry ferro-electric state, although the complexity of the crystal structure prevents a complete interpretation of the observed effects. In crystals of C_2 symmetry, all vibrations are Raman active while in D_{2d} symmetry all except one of the five vibrational symmetries are Raman active, so that no great change in the selection rules occurs between the para- and ferro-electric phases.

For the barium titanate structure however, the para-electric crystal symmetry is O_h with the five atoms in the unit cell all situated at centres of inversion, leading to four Raman-*inactive* optic modes, three of F_{1u} symmetry and one of F_{2u} symmetry. In the highest temperature ferro-electric phase the symmetry reduces to C_{4v} and the optic vibrations become first-order Raman-*active*, three of A_1 symmetry, one of B_1 symmetry and four of E symmetry. Barium titanate itself ($BaTiO_3$) has a transition temperature of 120°C and Bobovich and Bursian (1961) have measured its Raman spectrum in the ferro-electric tetragonal phase at room temperature. Only three Raman lines are observed and a complete interpretation is not possible. Bobovich and Bursian discuss the spectrum in terms of the normal vibrations of a Ti ion and its six O nearest neighbours. Ikegami (1964) has recently observed a larger number of lines in the Raman spectrum of $BaTiO_3$. The agreement between these two measurements is not very good. The Raman spectrum of strontium titanate ($SrTiO_3$) at room temperature has been measured by Narayanan and Vedam (1961). Strontium titanate may have a ferro-electric transition in the region of 35°K, but at room temperature it is para-electric with cubic O_h symmetry and is not expected to exhibit a first-order Raman spectrum. The peaks observed by Narayanan and Vedam must therefore be a second-order Raman spectrum, although the authors try to interpret their results as a first-order spectrum.

Of much greater value than either of the above experiments on the titanates would be a series of measurements of the Raman spectra at various temperatures above and below the transition temperature. The way in which a first-order Raman spectrum appears at the transition temperature could be determined and the variation of its intensity with temperature in the ferro-electric region would give an indication of the way in which the distortion of the lattice from its cubic structure varies with temperature. Above the transition temperature some of the low-frequency vibrations have a strongly temperature-dependent frequency (Cowley 1962) which could perhaps be investigated by the second-order Raman effect.

An attempt to observe effects of this type in NH_4HSO_4 and four other ferro-electrics has recently been made by Bazhulin *et al.* (1964). They measured Raman spectra at room temperature, and at lower temperatures in the regions of the ferro-electric transitions, but were unable to detect any low-frequency vibrations having markedly temperature-dependent frequencies.

2.6.6. *Rutile*

Titanium dioxide in the rutile structure is a fairly simple type of uniaxial crystal, having symmetry D_{4h} with two TiO_2 groups in the unit cell. The vibrational symmetries have been calculated by Dayal (1950), who finds that there are four Raman-active phonons, one each of symmetries A_{1g}, B_{1g}, B_{2g} and E_g.

The Raman spectrum of rutile has been investigated by Narayanan (1953) and Krishnamurti (1962). The latter author has assigned the four Raman-active phonon symmetries to four of the measured peaks, and has interpreted the remaining peaks as a second-order spectrum. This interpretation does not, however, seem to be altogether firmly established.

2.7. *Brillouin Scattering*

2.7.1. *Theory*

All the previous discussion has been concerned with Raman scattering from optic vibrations of the lattice. Acoustic lattice vibrations can also give rise to first-order Raman scattering. This effect was predicted by Brillouin (1922) and is sometimes referred to as Brillouin scattering. Consider the scattering arrangement shown in fig. 5, where **k** now refers to the wave vector of an acoustic phonon. For the Stokes component of the scattering the fractional shift in the frequency of the light is:

$$\frac{\omega_i - \omega_s}{\omega_i} = \frac{2\epsilon^{1/2} v}{c} \sin\frac{\psi}{2}, \quad . \; . \; . \; . \; . \; . \; . \; (67)$$

using (28) and energy conservation. Here v is the velocity of the acoustic phonon, i.e. the appropriate sound velocity. For the anti-Stokes component the sign of the right-hand side is reversed. Since v/c is typically of order 10^{-5}, the Brillouin shifts are very small, of order 2 or 3 cm^{-1} for many crystals. There are three acoustic branches having different values of v for a general direction of propagation, leading to three Stokes and three anti-Stokes components in the Brillouin spectrum. The Stokes and anti-Stokes peaks for a given branch have almost equal intensity due to the smallness of the phonon frequency. The main value of measurements of the Brillouin spectra lies in the fact that the elastic constants of a crystal can be determined from a knowledge of the acoustic phonon velocities.

The theory of Brillouin scattering can be derived from a classical macroscopic standpoint, by considering the elastic deformation produced in a crystal by a long-wavelength acoustic phonon. A strain e_{ij} in the lattice

produces a change in the component $\epsilon_{\mu\nu}$ of the optical dielectric constant tensor $\boldsymbol{\epsilon}$ given by:

$$\delta\epsilon_{\mu\nu} = -\sum_{\rho,\sigma}\epsilon_{\mu\rho}p_{\rho\sigma,ij}\epsilon_{\sigma\nu}e_{ij}, \quad . \quad . \quad . \quad . \quad . \quad . \quad . \quad (68)$$

where $p_{\rho\sigma,ij}$ is an elasto-optical coefficient (Nye 1957). Thus an acoustic phonon of frequency ω produces a component of the dielectric constant oscillating with the same frequency, and an incident light wave of frequency ω_i causes polarization components in the lattice having frequencies $\omega_i \pm \omega$. This oscillating polarization re-radiates energy at the frequencies $\omega_s = \omega_i \pm \omega$ of the Brillouin components. The strain components e_{ij} associated with an acoustic vibration are readily calculated and expressions for Brillouin scattering efficiencies can be obtained in terms of quantities which can be independently determined. In some respects the calculation of scattering by acoustic phonons is similar to that for polar scattering by optic phonons in a piezo-electric crystal. In the former case the optical dielectric constant ϵ is modulated by a strain wave via the elasto-optic effect, while in the latter case ϵ is modulated by a long-wavelength electric wave via the electro-optic effect.

A good account of the macroscopic calculation of the Brillouin scattering is given by Born and Huang (1954). For scattering by a cubic crystal with unpolarized incident light and with incident and scattered light along four-fold axes at right angles to each other, the scattering efficiencies for the three acoustic phonons are:

$$S_1 = \frac{k_B T \omega_s^4 \epsilon^4 L d\Omega}{64\pi^2 c^4}\left[\frac{p_{44}^2}{c_{44}}\right], \quad . \quad . \quad . \quad . \quad . \quad . \quad . \quad . \quad (69)$$

$$S_2 = 0, \quad . \quad . \quad . \quad . \quad . \quad . \quad . \quad . \quad . \quad . \quad . \quad . \quad . \quad . \quad . \quad (70)$$

$$S_3 = \frac{k_B T \omega_s^4 \epsilon^4 L d\Omega}{64\pi^2 c^4}\left[\frac{2(p_{44}^2 + p_{12}^2)}{c_{11} + c_{12} + 2c_{44}}\right], \quad . \quad . \quad . \quad . \quad . \quad (71)$$

where p_{ij} and c_{ij} are the elasto-optic coefficients and elastic constants in condensed notation (Nye 1957). It has been assumed that $k_B T \gg \hbar\omega$, and the Stokes and anti-Stokes components then have the same intensity. Note that the subsequent expressions given by Born and Huang on page 381 for scattering of polarized incident light by vibration 3 should be multiplied by a factor 2.

It is also possible to calculate the Brillouin scattering efficiencies using a microscopic model of the lattice. This has been attempted by Theimer (1951, 1952), who obtained results in disagreement with the above due to an error in his calculation (see the comments on p. 374 of Born and Huang 1954). The Brillouin scattering can also be calculated using a model in which the electron–lattice interaction is treated in the deformation potential approximation. This approach has been adopted by Loudon (1963 b) and the calculation is exactly analogous to that for Raman scattering by optic phonons outlined in §§ 2.2 and 2.4. The scattering tensor in the acoustic phonon case can be related to the elasto-optic

coefficients when the difference between ω_s and ω_i is ignored, and the final results of the calculation are in exact agreement with those of Born and Huang given in eqns. (69) to (71) above.

2.7.2. *Experiment*

Measurements of Brillouin spectra have generally been used to check already-known elastic constants rather than to obtain values of constants not previously known. An accuracy of about 1% can be achieved in Brillouin spectra measurements under favourable conditions. The first observation of this type of spectrum was made by Gross (1930) on quartz. Among subsequent measurements we may mention those of Krishnan on diamond (1947 a, b), fused quartz (1953) and LiF, NaCl, KCl, diamond, α-quartz, calcite ($CaCO_3$), alumina (Al_2O_3) and barite ($BaO \cdot SO_3$) (1955). The results of these measurements for the acoustic phonon velocities check reasonably well with values determined from the known elastic constants. Fused quartz, being an isotropic substance, possesses only two acoustic phonon velocities, for longitudinal and transverse sound waves, and should have two Brillouin peaks on either side of the exciting line. Only the longitudinal peak was detected by Krishnan (1953), but Flubacher *et al.* (1959) have also observed the much weaker transverse peak. Geiger and Kulp (1960) have reported a failure to observe Brillouin scattering in three types of quartz glass.

§ 3. Second-order Raman Effect

3.1. *Theory of the Scattering Process*

The first-order Raman effect is a scattering process in which a single phonon is either created or destroyed. In the second-order Raman effect, two phonons participate in the scattering process. They may both be created (giving a Stokes component in the scattered light) or one may be created and the other destroyed (giving a Stokes or anti-Stokes component) or finally both may be destroyed (giving an anti-Stokes component). There are two types of second-order Raman scattering and they give rise respectively to a line spectrum and a continuous spectrum.

The second-order line spectrum is due to processes in which light has suffered two successive first-order Raman scatterings. The process is illustrated in fig. 7, using the same notation as fig. 4. Figure 7 refers to the case in which the two phonons, having frequencies ω_0 and ω_0', are created. It is essential that first-order Raman scattering should be allowed for the two phonons individually, and the frequency shifts which occur in the second-order line spectrum are sums and differences of the shifts which occur in the first-order spectrum. It is not necessary for energy to be conserved in the intermediate state marked in fig. 7. However, the total wave vector in this state must be the same as in the initial state and this conservation law forces the wave vector of the first phonon (ω_0) to be small and

leads to the line nature of the resulting Raman spectrum. The second-order line spectrum provides no information about the phonon frequencies additional to that provided by the first-order spectrum, and we defer any further discussion to § 3.3.1, where an estimate is made of the relative intensities of the first and second-order Stokes lines in diamond. Since the process depends on two successive scattering events, which must both take place within the crystal volume, the scattering efficiency for the second-order line spectrum increases with the size of crystal.

Fig. 7

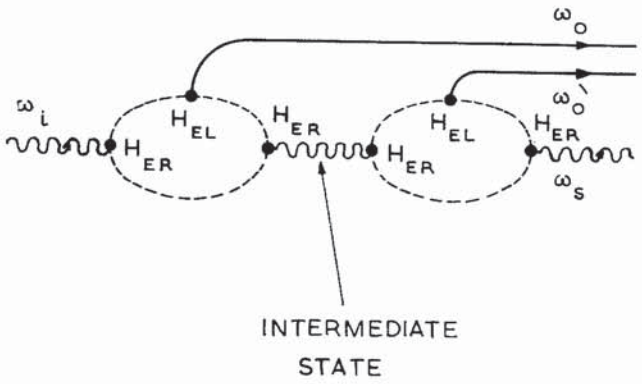

Elementary scattering process for the second-order line spectrum.

The remainder of this section is devoted to a discussion of the second-order continuous spectrum. The continuum is due to a scattering process in which the light interacts with a pair of phonons in a single event, as illustrated in fig. 8. We restrict our attention to the case where both

Fig. 8

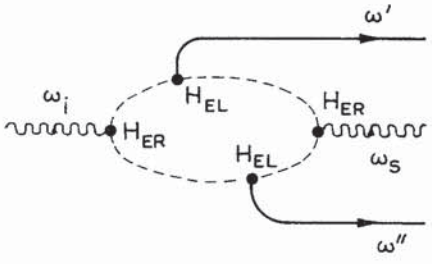

Elementary scattering process for the second-order continuous spectrum.

phonons are created. There is now no restriction on the phonon wave vectors other than the requirement that their sum should balance the change in wave vector of the scattered photon. Subject to this condition, the phonon wave vectors can range over the entire Brillouin zone. Since the photon wave vectors are negligible compared to the Brillouin zone

dimensions, wave vector conservation in this case requires effectively that the wave vectors of the two phonons should be equal and opposite. The continuous frequency distribution displayed by the scattered photons is thus proportional to a weighted density of lattice states in which two phonons of equal and opposite wave vector are present. The weighting is due to the frequency and wave vector dependence of the interactions involved in the scattering process. The second-order continuous spectrum results from a single scattering event and the scattering efficiency is therefore independent of the crystal size, as in the first-order Raman effect. This fact leads to an experimental means for resolving the second-order line and continuous spectra in cases where the continuum has sharp features or where the lines are broad.

The formal theory of the scattering efficiency for the second-order Raman effect can be tackled by the same methods as the first-order Raman effect. The first complete theoretical treatment was given by Born and Bradburn (1947), who applied their method to explain the experimental spectrum of NaCl. The same method was later applied to diamond by Smith (1948). The Born and Bradburn calculation of the second-order Raman effect is exactly analogous to their calculation of the first-order effect outlined in § 2.2. The scattered intensity is related to the electronic polarizability tensor, which must now be expanded as far as terms proportional to a product of two nuclear displacement amplitudes, i.e. the second-order Raman effect results from the term of order r^2 in (23). The final result of the general calculation can be cast in a form for the scattering efficiency at Raman shift ω analogous to (29), but with the square of the polarizability derivative replaced by complicated simultaneous summations over the squares of the polarizability second derivative components and over phonon pairs whose frequencies ω' and ω'' add to give ω. In the applications of the general theory to NaCl and diamond it was assumed for simplicity that only products of the nuclear displacements of nearest neighbours contribute to the second-order term in the electronic polarizability expansion, and that the dominant contribution to the density of states arises from the region of the Brillouin zone close to the centre of the hexagonal face. As a result of these approximations each pair of phonon branches makes a contribution to the second-order continuum intensity at frequency shift ω equal to the combined density of states of the two branches at frequency ω multiplied by a proportionality factor which is constant for a given pair of branches. In this way Born and Bradburn (1947) and Smith (1948) were able to extract some quantitative results from the general theory and show that Born's theory of lattice dynamics is able to account for the main features of the distribution of intensity in the second-order Raman spectra of NaCl and diamond.

It would also be possible to calculate the Raman scattering efficiency by treating the four-step scattering process illustrated in fig. 8 by fourth-order perturbation theory, similar to the treatment of first-order scattering